Chemical Physics Letters 595–596 (2014) 175–179

Contents lists available at ScienceDirect

Chemical Physics Letters

journal homepage: www.elsevier.com/locate/cplett

On the ferryl catalyst: Electronic structure and optimized *ab initio* geometry

U. Miranda [a], A.J.C. Varandas [a,*], I.G. Kaplan [b]

[a] Departamento de Química, and Centro de Química, Universidade de Coimbra, 3004-535 Coimbra, Portugal
[b] Instituto de Investigaciones en Materiales, Universidad Nacional Autónoma de México, Apdo. Postal 70-360, 04510 México, D.F., Mexico

ARTICLE INFO

Article history:
Received 20 December 2013
In final form 31 January 2014
Available online 7 February 2014

ABSTRACT

Full geometry optimizations have been carried out in order to determine the structure of the global minimum for the quintet state of the isolated α-center $[FeO]^{2+}$ using the neutral cluster $OFe(OH)_2$ as a model. The intrinsic reaction coordinate and a potential energy cut were calculated aiming at the examination of other low-energy structures. The absolute minimum here reported for the title species differs from the structures reported in other molecular orbital-based studies. Such a structure has been analyzed in order to determine the oxidation state of the Fe atom in the ferryl catalyst.

1. Introduction

The Fe/ZSM-5 catalyst became a subject of interest due to the selective oxidation of hydrocarbons by N_2O [1,2]; an example is the highly selective (around 95%) oxidation of benzene to phenol [2]. The catalytic activity is related to the Fe^{2+} species [3]. An oxidative center, $[FeO]^{2+}$, is formed during the decomposition of N_2O on the active sites [3–5] of the Fe/HZSM-5 system:

$$N_2O + Fe^{2+} \rightarrow [FeO]^{2+} + N_2$$

The α-oxygen species so formed are very reactive in oxidation reactions [2,4,5] but tend to be stable in the absence of reagents. This α-oxygen center, $[FeO]^{2+}$, is bonded to the zeolite through O or OH groups. It can be described using the valence bond schemes $Fe^{IV} = O$ and $Fe^{III} - O^{\cdot -}$[closecurl]; however, these are different states of the α-oxygen center rather than resonance structures, and hence it is unknown which of them is found under catalytic conditions [2,6–9]. Many studies [5,10–13] have been performed aiming at the determination of the oxidative state of the Fe atoms. Despite the evidence provided by resonant inelastic X-ray spectroscopy [14] of the presence of $Fe^{III} - O^{\cdot -}$ in the α-oxygen center, there is no certainty concerning the state that compels an oxidative reaction. For this reason, it is very important to determine the electronic structure of the $[FeO]^{2+}$ system.

A large number of studies has been performed using density functional theory [10,15,16]; however, the results obtained with this single-determinant approach are in many cases not reliable, especially for 3*d* transition metal compounds (see the review by Cramer and Truhlar [17], and the analysis of this problem by Kaplan [18,19]). Note that even the simplest 3*d*-electron systems, dimers, can only be precisely calculated by the multireference configuration interaction method [20,21] (indeed, we should emphasize that single-reference MO methods face severe problems in describing 3*d*-systems).

The oxidation state of Fe in an α-center has been suggested from experimental work to be +2 [22,23]. Assuming that ferrous iron in zeolites is qualitatively equivalent to free iron coordinating two OH groups (which usually withdraw almost two electrons from the iron atom), Zilberberg et al. [6] carried out calculations to study the electronic structure of atomic oxygen adsorbed in the ferrous α-center Fe(II)–O using $OFe(OH)_2$ as a neutral model of $[FeO]^{2+}$. They have performed complete-active-space self-consistent-field (CASSCF [24]) calculations using (10e,9o) as the active space, which consists of the 3*d* and 4*s* orbitals of Fe and the 2*p* orbitals of O. The dynamical correlation was further obtained by the multiconfigurational quasi-degenerate perturbation theory (MCQDPT) [25,26] as well as DFT/B3LYP [27,28] calculations. CASSCF optimized geometries of all states have been reported, as well as constrained CASSCF potential energy scans, with the ground state of $OFe(OH)_2$ being predicted [6] to be $^5A_1$. Analogous scans were obtained using MCQDPT corrections using CASSCF optimized geometry for various states. The above authors [6] have further given an analysis of the occupancies of the natural orbitals for all the states and presented the main electron configuration for the bonding. They concluded that there are three covalent bonds of the σ and π types involving the oxygen and ferrous iron. In addition, potential energy curves were reported [6] for all states, with the $^5A_1$ state shown to dissociate to $O^- + Fe(OH)^{2+}$ based on the occupancies of the natural orbitals. Upon such an analysis, it was concluded that the electron

* Corresponding author.
E-mail address: varandas@uc.pt (A.J.C. Varandas).

http://dx.doi.org/10.1016/j.cplett.2014.01.056
0009-2614/

configuration in the dissociation limit corresponds to $Fe^{3+} + O^{-}$. Optimized geometries were also given [6] for the various states (triplets, quintets, and septets).

All structures presented in Ref. [6] are planar and symmetrical with respect to the H atoms; see structure (a) in Figure 1. The C_{2v} symmetry has been assumed [6,8] in all calculations, thus implying the equivalence of the two bridged oxo centers which bind the iron center to the zeolite lattice.

In order to obtain optimized geometries with multi-reference perturbation theory calculations, Malykhin et al. [8] published a further study using the same $OFe(OH)_2$ model: they applied the fully optimized reaction space (FORS) variant of CASSCF theory [29] and the intruder-state-avoidance multireference perturbation theory (ISA-MRPT) [30] method. The active space, (10*e*,10*o*), included the five 3*d* orbitals of the iron atom, three 2*p* orbitals of oxygen and two diffuse-like orbitals. The authors [8] carried out geometry optimizations for triplet, quintet and septet states with ISA-MRPT. They reported the same ground state, $^5A_1$ and compared the results obtained for this state with the other low-lying one $^5B_2$. The optimized geometry for the ground state is structure (a) in Figure 1; it is the same geometry as reported in Ref. [6]. However, Malykhin et al. [8] proposed yet another structure, Figure 1b, to analyze the influence of the geometry on the electronic structure of the active species.

The authors [8] anticipated that the ground state should be $^5A_1$ at the employed CASSCF and ISA-MRPT levels of theory if structure (b) of Figure 1 were used instead of (a). The same C_{2v} symmetry restriction has been used [8].

It should be mentioned that for transition metal compounds the CASPT2 method can predict an artificial stability [31]; this approach and even the more sophisticated multireference *n*-electron valence state perturbation theory (NEVPT) [32] approach do not give a reliable Mulliken population, see discussion in Ref. [21].

In this Letter, we report the results obtained for the above $OFe(OH)_2$ neutral model of the isolated α-center $[FeO]^{2+}$ using the CASSCF and multireference configuration interaction (MRCI) methods. It is worthwhile noting that the real geometry of the α-center is still unknown, since in all published calculations the crystal field of zeolite was not taken into account.

2. Methodology

We have used here the same molecular model, namely $OFe(OH)_2$. The methods employed were CASSCF [33,34] and MRCI [35,36] with the Dunning-type cc-pV*X*Z ($X = 3, 4$) basis set of Balabanov and Peterson [37] and smaller basis sets: 6–31G** for Fe [38], 6–31G* for O [39] and 6–311G** for H [39], named hereinafter 6–31G* for the sake of brevity. The active space (10*e*,9*o*) is defined by the 4*s* and 3*d* orbitals of Fe and the 2*p* orbitals of O. Full geometry optimizations (all 12 parameters were taken into account) have been performed without symmetry restrictions for the lowest energy structure and transition state of the quintet molecular term; the intrinsic reaction coordinate (IRC) calculations were also performed. Both the geometry optimizations and IRC calculations were done using the quadratic steepest descent (QSD) optimization method of Sun and Ruedenberg [40] at both CASSCF/6–31G* and CASSCF/cc-pV*X*Z levels of theory. The CASDC (an abbreviation of CASSCF and dynamical correlation) scheme proposed by Varandas [41], which follows from the partition $E_{MRCI} = E_{CAS}(r) + E_{dc}(r)$ of the molecular energy, was followed for the IRC calculations. This is based on a four point premise [41,42]:

1. Bond-breaking/bond-forming reactions are best treated by multireference methods such as MRCI, preferably when the Davidson correction Q [43,44] is added, MRCI + Q.
2. A convenient reference for MRCI is the full-valence-complete-active-space (FVCAS) wave function, warranting in principle a correct description at dissociation.
3. Can be described by a single reactive coordinate.
4. Single-point MRCI + Q calculations along the optimized FVCAS path should differ marginally from the unaffordable directly optimized MRCI + Q ones.

The results obtained in smaller systems [41,42] are accurate, and hence we also expect reliable results from the present calculations which are not too computationally demanding, an attribute that might be extreme for the system here studied. Nevertheless, the minimum was optimized at both MRCI/6–31G* and MRCI/cc-pVTZ levels of theory. The convergence criteria used for the optimizations and the IRC calculations were 10^{-6} for the gradient and 10^{-8} for the energy in all CASSCF calculations; for the MRCI optimizations of the minimum, the convergence criteria were 10^{-4} for the gradient and 10^{-6} for the energy. The harmonic vibrational frequencies were also calculated. The MRCI energies are corrected by means of the Davidson scheme [43,44], in order to approximately correct for quadruple electronic excitations and diminish size-inconsistency. All calculations were carried out with the MOLPRO [45,46] suite of programs.

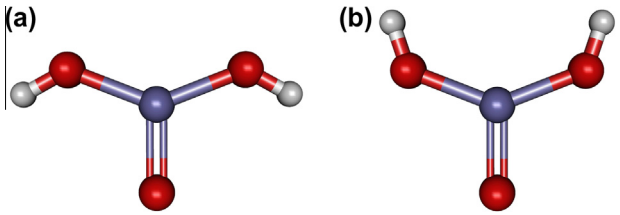

Figure 1. The conformations of $OFe(OH)_2$ obtained in Refs. [6,8]. The central atom of the structures is Fe (dark gray color), oxygen atoms are in red color and H atoms in white. Structure (a) is the geometry reported in both studies as the ground state. Structure (b) was proposed in Ref. [8] as another model to study the influence on geometry on the electronic structure.

3. Results

3.1. Geometry optimization

We have calculated the optimized geometries of both the minimum and transition states. For the former, the structures obtained are planar irrespectively of basis set, except for the structure of the transition state, where one of H atoms is out of the plane; the values of the involved dihedral angles are $\theta_3 = 247.68$, 261.99 and 258.53°, with the 6–31G*, cc-pVTZ and cc-pVQZ basis sets, respectively. The transition state structure was optimized only at the CASSCF level of theory. In Table 1 all optimized parameters obtained with the CASSCF method and various basis sets are presented, while Figure 2 shows the structures obtained. In all the presented plots, the central atom is Fe; as usual, O atoms are in red, H atoms in white.

The minimum has also been MRCI optimized with the 6–31G* and cc-pVTZ basis. The bond distance Fe–O in the α-oxygen center is shorter at the MRCI level than at the CASSCF one. All other bond distances remain essentially unaltered in both methods. The angles are slightly modified but the structures remain planar. The parameters obtained from the MRCI optimization of the minimum are presented in Table 2.

Harmonic frequencies and total energies for both the minimum and transition states are presented in Table 3. The optimized geometry of the minimum is planar and not symmetric with respect to the OH bonds, in contrast to the structures presented

Table 1
Optimized geometry parameters for the minimum and the transition state at CASSCF/6–31G*; cc-pV*X*Z level of theory. Bond distances (r_i) are in Å; angles (α_i) and dihedrals (θ_i) are in degrees.

	Minimum			Transition state		
	6-31G*	cc-pVTZ	cc-pVQZ	6-31G*	cc-pVTZ	cc-pVQZ
r_1	1.78	1.80	1.80	1.80	1.80	1.80
r_2	1.79	1.80	1.80	1.78	1.81	1.81
r_3	0.94	0.94	0.93	0.94	0.94	0.93
r_4	1.79	1.80	1.81	1.79	1.80	1.80
r_5	0.94	0.94	0.93	0.94	0.93	0.93
α_1	120.0	119.7	119.4	117.4	117.4	117.3
α_2	129.8	128.6	128.9	133.2	128.7	128.9
α_3	119.6	120.0	120.2	118.7	120.0	119.9
α_4	227.8	130.9	131.0	138.6	142.8	142.8
θ_1	180.0	177.9	177.4	187.2	180.6	185.1
θ_2	180.0	178.1	177.6	180.5	179.2	183.6
θ_3	180.0	1.3	1.7	247.7	262.0	258.5

[a] r_1 is the bond distance of Fe–O.
[b] r_2 and r_4 are the two bond distances Fe–OH.
[c] r_3 and r_5 are the two bond distances O–H.
[d] α_1 and α_3 are the two angles O–Fe–OH.
[e] α_2 and α_4 are the two angles Fe–O–H.
[f] θ_1 and θ_3 are the two dihedral angles H–O–Fe–O.
[g] θ_3 is the dihedral angle (H–) O–OFe–O (–H).

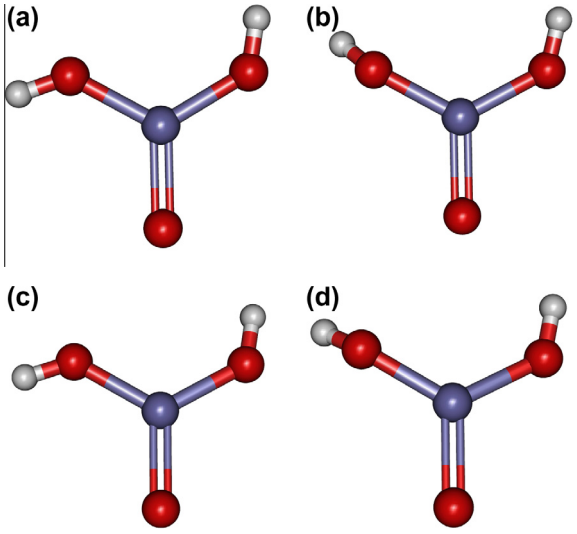

Figure 2. Structures of the minimum (a) and transition state (b) optimized with the 6–31G* basis sets and structure of the minimumm (c) and transition state (d) optimized with the cc-pV*X*Z (where $X = 3, 4$) basis sets. The transition state structures were optimized both at CASSCF/6–31G* and CASSCF/cc-pV*X*Z levels of theory, while the structures of the minimum were optimized at CASSCF and MRCI levels with the 6–31G* and cc-pVTZ basis.

Table 2
Optimized geometry parameters for the minimum at MRCI/6–31G* and MRCI/cc-pVTZ levels of theory. Bond distances (r_i) are in Å, angles (α_i) and dihedrals (θ_i) in degrees.

	6-31G*	cc-pVTZ
r_1	1.65	1.73
r_2	1.79	1.81
r_3	0.94	0.94
r_4	1.79	1.81
r_5	0.94	0.94
α_1	127.1	122.9
α_2	136.9	127.4
α_3	107.0	117.1
α_4	125.0	128.1
θ_1	180.0	180.5
θ_2	180.0	180.3
θ_3	0.0	−1.0

Table 3
Calculated total energy (in E_h after adding 1488 E_h) and harmonic frequency (cm^{-1}) for the ground state and transition state of $OFe(OH)_2$.

Basis set	Minimum				Transition state	
	CASSCF		MRCI		CASSCF	
	E	ω_e	*E*	ω_e	*E*	ω_e
6–31G*	−0.077178	133.28	−0.215419	115.54	−0.068468	182.46
cc-pVTZ	−0.351690	164.77	−0.555684	102.22	−0.348728	176.20
cc-pVQZ	−0.374251	166.99			−0.371264	177.22

in Refs. [6,8]. The convergence criteria employed in our calculations were tight, which gives reliability to the results obtained.

3.2. Intrinsic reaction coordinate

Because our optimized structure for the minimum differed from the previously reported [6,8], we have performed IRC calculations to determine the path that might lead to the lowest energy structure. Thence, we have calculated the IRC at both the CASSCF/6–31G* (see Figure 3) and the CASSCF/cc-pVQZ (see Figure 4) levels of theory, followed by MRCI/6–31G* and MRCI/cc-pVQZ single point calculations for the local minimum, transition state and global minimum structures. The predicted geometry of the local minimum is planar and it has both H atoms symmetrically placed in the opposite direction to the α-oxygen center, while the structures of the transition state and global minimum are the same as the ones obtained via geometry optimization. Starting from the local minimum in the IRC, one of the symmetrically placed hydrogen atoms moves out of the plane until the transition state structure and then continues moving until the global minimum, where the H atom is again in the molecular plane.

Table 4 gives the calculated total energy for each of the three structures (local minimum, transition state and global minimum) of the IRC calculated with the 6–31G* (Figure 3) and cc-pVQZ (Figure 4) basis sets. As can be seen from both IRC plots, the structure of the local minimum corresponds to structure (b) proposed in Ref. [8] (see Figure 1).

As shown, the difference between the MRCI/6–31G* energies of the two minima is of 1.1 kcal mol^{-1}; the difference between the local minimum and the transition state is 0.73 kcal mol^{-1} and between the global minimum and the transition state is 1.82 kcal mol^{-1}. The energy difference between the two minima

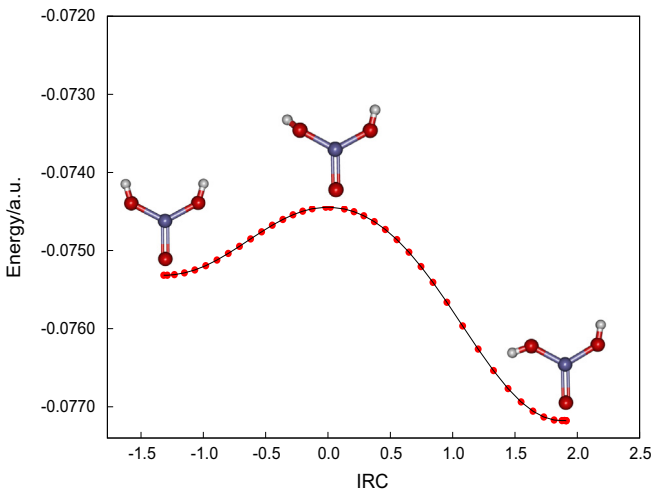

Figure 3. Intrinsic reaction coordinate for $OFe(OH)_2$ system calculated at the CASSCF/6–31G* level of theory. The three structures corresponding to the local minimum, transition state and global minimum were also calculated at the MRCI/6–31G* level of theory.

Table 4
Total energies (in E_h after adding 1488 E_h) of the local and global minima and the transition state of $OFe(OH)_2$ calculated at the CASSCF/MRCI + Q level using the 6–31G* and cc-pVQZ basis sets. These structures correspond to those shown in the IRC in Figures 3 and 4.

Structure	CASSCF	MRCI	+Q
*6–31G**			
Local minimum	−0.075316	−0.211444	−0.217165
Transition state	−0.074445	−0.210283	−0.215984
Global minimum	−0.077178	−0.213192	−0.218889
cc-pVQZ			
Local minimum	−0.373003	−0.590387	−0.601032
Transition state	−0.371141	−0.588467	−0.599115
Global minimum	−0.374251	−0.591348	−0.601948

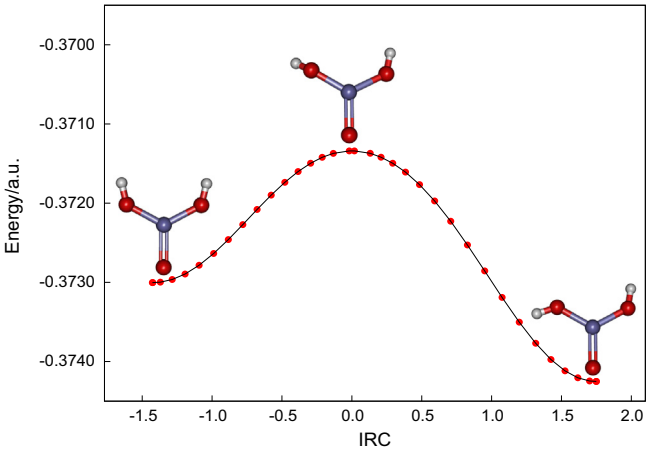

Figure 4. Intrinsic reaction coordinate for $OFe(OH)_2$ system calculated at the CASSCF/cc-pVQZ level. The three structures corresponding to the local minimum, transition state and global minimum were also calculated at the MRCI/cc-pVQZ level of theory.

at the MRCI/cc-pVQZ level of theory is 0.6 kcal mol^{-1}; between the local minimum and the transition state is 1.2 kcal mol^{-1} and between the global minimum and the transition state is 1.8 kcal mol^{-1}. Note that one or both of the H atoms can move out of the plane in the IRC.

We calculated also the potential-energy surface (PES) at the CASSCF/6–31G* level, keeping fixed all the geometry parameters except of the two Fe-O- H angles (α_2 and α_4). Even though the transition state obtained from the geometry optimizations and the IRC calculation is not planar, all calculations for this cut of the PES have been carried maintaining for simplicity the planar geometry. Our goal in obtaining this PES cut was to understand and corroborate the transformation of the structure of the quintet state studied through the modification of the two Fe–O–H angles. Figure 5 shows that the absolute minimum corresponds to the structure reported in Table 1 and illustrated in Figure 2, while the minima reported in Refs. [6,8] are actually local minima.

For $\alpha_2 = 228^\circ$, on the left side of Figure 5, we can see a symmetric structure which corresponds to the one reported in previous studies [6,8] (see structure (a) in Figure 1); in this structure the other angle is $\alpha_4 = 132^\circ$. Following the direction of increasing angle α_4, we see the transition state, where the H atoms are placed at angles of $\alpha_2 = 228^\circ$ and $\alpha_4 = 176^\circ$. The last structure on the path corresponds to the global minimum, where $\alpha_2 = 228^\circ$ and $\alpha_4 = 230^\circ$. For $\alpha_2 = 228^\circ$, starting from rigth to left, one has the path corresponding approximately to the IRC (see Figures 4 and 5); recall that the IRC involves nonplanar structures.

The energies of the two local minima obtained from MRCI/6–31G* calculations are in Table 5. Note that the energy of the local

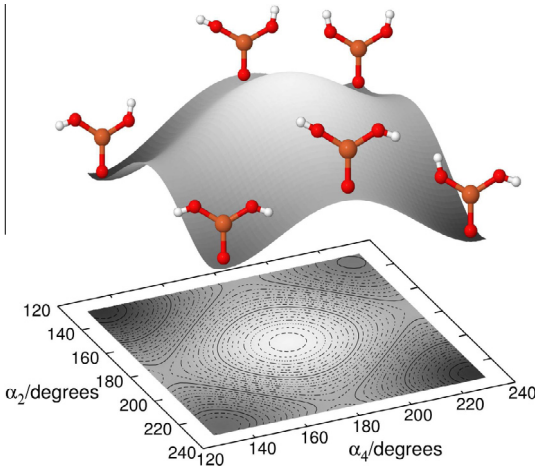

Figure 5. Potential energy surface calculated at the CASSCF/6–31G* level of theory by varying only the two angles of Fe–O–H of the $OFe(OH)_2$ system. All calculations were performed on planar structures and the remaining parameters were kept fixed in order to simplify the problem.

minimum here calculated (I in Table 5) is lower than the energy of the structure reported in the previous publications [6,8] (structure (a) in Figure 1, referred to as II in Table 5).

3.3. Population analysis

It has been suggested [3] that during the oxidation reactions performed with N_2O, Fe^{2+} is oxidized to its trivalent state when the α-oxygen is formed. This stoichiometric reaction is written as follows:

$$N_2O + Fe^{2+} \xrightarrow{250\ ^\circ C} Fe^{3+}O^- + N_2$$

Our natural atomic orbitals (NAO) results in Table 6 show a negative charge of −0.69 on α-oxygen, mostly on the 2*p* orbitals. This charge is transferred from the 3*d* orbitals of Fe atom. Each OH in the system receives a charge transfer of −0.8. In this way, the Fe atom has a positive charge of +2.29. These numbers differ somewhat from the reaction scheme shown above, although this is probably due to having satisfied stoichiometry in that scheme by considering charges only in the Fe and O atoms. The Mulliken population analysis gives similar results.

The NAO results corresponding to the local minima, hardly change (see Table 7) with respect to those of the global minimum shown in Table 6. The positive charge on the Fe atom is increased by 0.07 in one local minimum [structure (a) of Figure 1] and by 0.02 in the other [structure (b)], but are minor. As the electron structure is not altered in any of the three structures, the electron distribution remains almost the same for the different geometries. This can also be observed from the highest occupied molecular orbital (HOMO) and lowest unnoccupied (LUMO) one, which are equal at the global minimum, transition state and local minimum, as shown in Figure 6.

Table 5
Total energy (in E_h after adding 1488 E_h) values of the two local minima shown in the PES of Figure 5. Structure II corresponds to structure (a) in Figure 1, which was reported as the ground state geometry in Refs. [6,8], while structure I corresponds to structure (b) reported also in Ref. [8].

	CASSCF	MRCI	+Q
Structure I	−0.075096	−0.211187	−0.216906
Structure II	−0.069994	−0.173257	−0.176787

Table 6
Natural atomic orbitals occupations for the minimum calculated at the MRCI/cc-pVTZ level of theory.

Unique atom	*s*	*p*	*d*	*f*	*g*	Total	Charge
α-O	3.96	4.72	0.01	0.0	0.0	8.69	−0.69
Fe	6.23	12.04	5.44	0.0	0.0	23.71	+2.29
O	3.81	5.47	0.01	0.0	0.0	9.29	−1.29
H	0.51	0.0	0.0	0.0	0.0	0.51	+0.49
O	3.81	5.46	0.01	0.0	0.0	9.28	−1.28
H	0.52	0.0	0.0	0.0	0.0	0.52	+0.48

Table 7
Natural atomic orbitals occupations for the two local minima, corresponding to structures (a) and (b) in Figure 1, calculated at the MRCI/cc-pVTZ level of theory.

Unique atom	*s*	*p*	*d*	*f*	*g*	Total	Charge
Local minimum corresponding to structure (a) in Figure 1							
O	3.97	4.79	0.01	0.0	0.0	8.77	−0.77
Fe	6.23	12.04	5.37	0.0	0.0	23.64	+2.36
O	3.81	5.46	0.01	0.0	0.0	9.28	−1.28
H	0.51	0.00	0.0	0.0	0.0	0.51	+0.49
O	3.81	5.47	0.01	0.0	0.0	9.29	−1.29
H	0.51	0.00	0.0	0.0	0.0	0.51	+0.49
Local minimum corresponding to structure (b) in Figure 1							
O	3.96	4.74	0.01	0.0	0.0	8.71	−0.70
Fe	6.24	12.04	5.41	0.0	0.0	23.69	+2.31
O	3.81	5.47	0.01	0.0	0.0	9.29	−1.29
H	0.51	0.0	0.0	0.0	0.0	0.51	+0.49
O	3.81	5.47	0.01	0.0	0.0	9.29	−1.29
H	0.51	0.0	0.0	0.0	0.0	0.51	+0.49

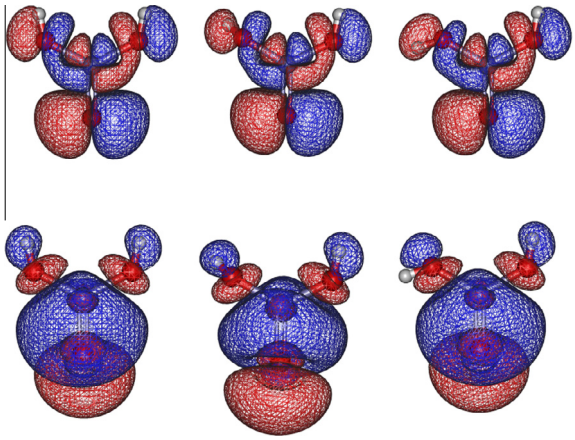

Figure 6. The HOMO and LUMO orbitals of the three structures (from left to right, local minimum, transition state and global minimum) obtained in the IRC calculations.

4. Conclusions

The geometry of the lowest-energy quintet state is not completely symmetric and is not completely planar, in contrast to previous studies [6,8]. The optimizations were carried out including the 12 parameters and with no symmetry restrictions, which together with the rigorous convergence criteria used in the geometry optimizations and the IRC calculations, allow us to conclude that the structures for the isolated ferril catalyst presented in previous studies are not the lowest energy ones. The PES obtained using planar geometries confirms the results mentioned above. According to the NAO population results from the present Letter, the charge of the Fe atom is +2.29 and the one of oxygen is −0.69, and so the alfa-center [OFe] has a charge of +1.6 which is approximately the accepted value of +2, although the oxidation state of the Fe atom lies closer to Fe(II) than to Fe(III). The atomic charges as well as the frontier orbitals do not change in any of the different geometries found in the calculations because the electron structure does not undergo any significant modification.

Acknowledgments

This Letter is supported by FEDER through "Programa Operacional Factores de Competitividade - COMPETE" and national funds under the auspices of Fundação para a Ciência e a Tecnologia, Portugal (contracts PTDC/QEQ-COM/3249/2012 and PTDC/AAG-MAA/4657/2012), with the calculations carried out at the Coimbra T&CC cluster. U.M. wishes to express his gratitude also to Consejo Nacional de Ciencia y Tecnología, México, for posdoctoral grant 177419 and Rahul Sharma for useful discussions.

References

[1] G. Panov, CATTECH 4 (2000) 18.
[2] G.I. Panov, A.K. Uriarte, M.A. Rodkin, V.I. Sobolev, Catal. Today 41 (1998) 365.
[3] G.I. Panov, K.A. Dubkov, E.V. Starokon, Catal. Today 117 (2006) 148.
[4] V. Sobolev, K. Dubkov, O. Panna, G. Panov, Catal. Today 24 (1995) 251.
[5] K. Dubkov, V. Sobolev, E. Talsi, M. Rodkin, N. Watkins, A. Shteinman, G. Panov, J. Mol. Catal. A: Chem. 123 (1997) 155.
[6] I. Zilberberg, R.W. Gora, G.M. Zhidomirov, J. Leszczynski, J. Chem. Phys. 117 (2002) 7153.
[7] J. Jia, Q. Sun, B. Wen, L. Chen, W. Sachtler, Catal. Lett. 82 (2002) 7.
[8] S. Malykhin, I. Zilberberg, G. Zhidomirov, Chem. Phys. Lett. 414 (2005) 434.
[9] M.J. Louwerse, E. Jan, Phys. Chem. Chem. Phys. 9 (2007) 156.
[10] N. Kachurovskaya, G. Zhidomirov, E. Hensen, R. van Santen, Catal. Lett. 86 (2003) 25.
[11] G. Berlier, F. Bonino, A. Zecchina, S. Bordiga, C. Lamberti, ChemPhysChem 4 (2003) 1073.
[12] E. Hensen, Q. Zhu, R. van Santen, J. Catal. 220 (2003) 260.
[13] E.V. Starokon, M.V. Parfenov, L.V. Pirutko, S.I. Abornev, G.I. Panov, J. Phys. Chem. C 115 (2011) 2155.
[14] G.D. Pirngruber, J.D. Grunwaldt, P.K. Roy, J.A. van Bokhoven, O. Safonova, P. Glatzel, Catal. Today 126 (2007) 127.
[15] K. Yoshizawa, Coord. Chem. Rev. 226 (2002) 251.
[16] A. Rosa, G. Ricciardi, E.J. Baerends, Inorg. Chem. 49 (2010) 3866.
[17] C.J. Cramer, D.G. Truhlar, Phys. Chem. Chem. Phys. 11 (2009) 10757.
[18] I.G. Kaplan, Int. J. Quantum Chem. 107 (2007) 2595.
[19] I.G. Kaplan, Int. J. Quantum Chem. 112 (2012) 2858. Section 3.
[20] D. Tzeli, U. Miranda, I.G. Kaplan, A. Mavridis, J. Chem. Phys. 129 (2008) 154310.
[21] U. Miranda, I.G. Kaplan, Eur. Phys. J. D 63 (2011) 263.
[22] K.A. Dubkov, N.S. Ovanesyan, A.A. Shteinman, E.V. Starokon, G.I. Panov, J. Catal. 207 (2002) 341.
[23] E.V. Starokon, K.A. Dubkov, L.V. Pirutko, G.I. Panov, Top. Catal. 23 (2003) 137.
[24] B.O. Roos, Adv. Chem. Phys. 69 (1987) 399.
[25] H. Nakano, J. Chem. Phys. 99 (1993) 7983.
[26] H. Nakano, Chem. Phys. Lett. 207 (1993) 372.
[27] A.D. Becke, J. Chem. Phys. 98 (1993) 1372.
[28] C. Lee, W. Yang, R.G. Parr, Phys. Rev. B 37 (1988) 785.
[29] B.R. Brooks, J. Chem. Phys. 70 (1979) 5092.
[30] H.A. Witek, Y.-K. Choe, J.P. Finley, K. Hirao, J. Comput. Chem. 23 (2002) 957.
[31] A.A. Buchachenko, G. Chałasiński, M.M. Szcześniak, J. Chem. Phys. 132 (2010) 024312.
[32] C. Camacho, H.A. Witek, R. Cimiraglia, J. Chem. Phys. 132 (2010) 244306.
[33] H.-J. Werner, P.J. Knowles, J. Chem. Phys. 82 (1985) 5053.
[34] P.J. Knowles, H.-J. Werner, Chem. Phys. Lett. 115 (1985) 259.
[35] H.-J. Werner, P.J. Knowles, J. Chem. Phys. 89 (1988) 5803.
[36] P.J. Knowles, H.-J. Werner, Chem. Phys. Lett. 145 (1988) 514.
[37] N.B. Balabanov, K.A. Peterson, J. Chem. Phys. 123 (2005) 064107.
[38] V.A. Rassolov, J.A. Pople, M.A. Ratner, T.L. Windus, J. Chem. Phys. 109 (1998) 1223.
[39] R. Krishnan, J.S. Binkley, R. Seeger, J.A. Pople, J. Chem. Phys. 72 (1980) 650.
[40] J.-Q. Sun, K. Ruedenberg, J. Chem. Phys. 99 (1993) 5257.
[41] A.J.C. Varandas, J. Phys. Chem. A 117 (2013) 7393.
[42] A.J.C. Varandas, J. Chem. Theory Comput. 8 (2012) 428.
[43] S.R. Langhoff, E.R. Davidson, Int. J. Quantum Chem. 8 (1974) 61.
[44] E.R. Davidson, D.W. Silver, Chem. Phys. Lett. 52 (1977) 403.
[45] H.-J. Werner, P.J. Knowles, G. Knizia, F.R. Manby, M. Schütz, WIREs Comput. Mol. Sci. 2 (2012) 242.
[46] H.-J. Werner, P.J. Knowles, G. Knizia, F.R. Manby, M. Schütz, et al., Molpro, version 2010.1, a package of ab initio programs, 2010. http://www.molpro.net.